Graphene Oxide-Arginine Composites: Efficient Dual Function Materials for Integrated CO2 Capture and Conversion

Graphene Oxide-Arginine Composites: Efficient Dual Function Materials for Integrated CO_2 Capture and Conversion

Sebastiano Mantovani,[a,b] Angela Pintus,[b] Alessandro Kovtun,[b] Angela Gondolini,[c] Simone Casadio,[c,d] Alessandra Sanson,[c] Tainah D. Marforio,[a,e] Matteo Calvaresi,[a,e] Marzio Rancan,[f] Lidia Armelao,[d,g] Giulio Bertuzzi,[a,e] Manuela Melucci,*[b] and Marco Bandini*[a,e]

[a] Mr. S. Mantonvani, Dr. T.D. Marforio, Prof. M. Calvaresi, Dr. G. Bertuzzi, Prof. M. Bandini, Dipartimento di Chimica "Giacomo Ciamician", Alma Mater Studiorum – Università di Bologna, via Gobetti 85, 40129, Bologna, Italy
E-mail: marco.bandini@unibo.it

[b] Mr. S Mantovani, Mrs A. Pintus, Dr. A. Kovtun, Dr. M. Melucci, The Institute for Organic Synthesis and Photoreactivity (ISOF), National Research Council (CNR), Via P. Gobetti 101, 40129 Bologna, Italy
E-mail: manuela.melucci@isof.cnr.it

[c] Dr. A. Gondolini, Dr. S. Casadio, Dr. A. Sanson, Institute of Science, Technology and Sustainability for Ceramics (ISSMC, former ISTEC), National Research Council (CNR), via Granarolo, 64, 48018, Faenza (RA), Italy

[d] Dr. S. Casadio, Prof. L. Armelao, Department of Chemical Sciences, University of Padova, Via Marzolo 1, 35131 Padova, Italy

[e] Prof. M. Calvaresi, Dr. G. Bertuzzi, Prof. M. Bandini, Center for Chemical Catalysis - C^3, Alma Mater Studiorum – Università di Bologna, via Gobetti 85, 40129, Bologna, Italy

[f] Dr. M. Rancan, Institute of Condensed Matter Chemistry and Technologies for Energy (ICMATE), National Research Council (CNR), c/o Department of Chemical Sciences, University of Padova, Via Marzolo 1, 35131, Padova, Italy

[g] Prof. L. Armelao, Department of Chemical Sciences and Materials Technologies (DSCTM), National Research Council (CNR), Piazzale Moro 7, 00185, Roma, Italy

Abstract: The "on-demand" capture and utilization of CO_2 is effectively realized with a readily accessible dual function organic composite. The covalent and controlled derivatization of graphene oxide (GO) surface with naturally occurring arginine led to a "smart" material capable of capturing (chemisorption) CO_2 from high-purity flue-gas as well as low-concentration streams (*i.e.* direct air capture) and concomitant chemical activation toward the incorporation into cyclic carbonates. The overall integrated CO_2 capture and conversion (ICCC) strategy has been fully elucidated mechanistically via dedicated computational, spectroscopic and thermal analyses.

Introduction

Climate change is one of the world's most pressing challenges. Human emissions of greenhouse gases have increased global temperatures by around 1 °C since pre-industrial times.[1] In particular, a rapid rise in global CO_2 concentrations (above 400 ppm with prediction of 500 ppm levels at the end of this century in absence of effective mitigation plans) has been monitored over the past few centuries and in recent decades. While the planet struggles to absorb this excess carbon, we as a global community must systemically and aggressively adapt our economies to reduce further carbon pollution, to keep our planet from warming.[2] However, we should be aware that, the largest part of the manufactures that we daily face are made on carbon, therefore, a carbon-free chemical industry is somehow considered utopistic. Accordingly, the current global challenge relies on the discovery of eco-innovations (materials, energy sources, technologies…) to support a sustainable socioeconomic scenario.

In this context, the mitigation of CO_2 accumulation in the atmosphere is a current world-wide scientific *hot topic* in order to tackle environmental degradation phenomena.[3] Here, an intense CCS (CO_2 Capture and Storage/Removal) program has started a few decades ago.[4] However, despite the availability of numerous emerging technologies mainly addressing post-combustion strategies,[5] its use is still suffering of serious limitations deriving from high costs and intensive energy requirements for separation, pumping and housing/burying of CO_2.[6] Additionally, the strategy does not valorize CO_2 directly with a concrete risk of leakage.[7] CCS technologies are now paralleled by the carbon dioxide capture, utilization and storage approach (CCUS) that consists in three different steps, namely: the separation of CO_2 from emission sources, transportation and CO_2 conversion-utilization (Figure 1-upper).[8]

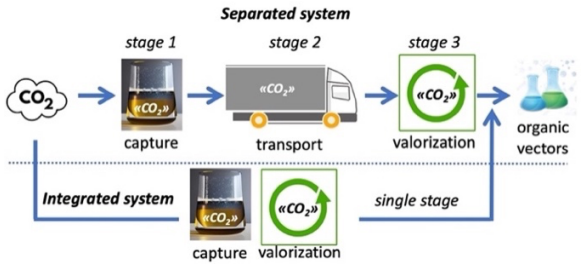

Figure 1. Schematic representation of a model CCUS approach (upper) and ICCC (lower).

CCUS is getting growing credit world-wide and is organized in protocols embracing the "direct" use of pure CO_2 (carbonated drinks, fire extinguishers, etc.) or "indirect" CO_2 utilization,

addressing the conversion of CO_2 into new fuels,[9] materials and chemical commodities.[10] The latter approach also inspired the scientific community towards the development of energetically efficient CO_2 conversion methods based on chemo-, electro- or photo-catalysis and their combination.

In this context, "integrated CO_2 capture and conversion (ICCC)" is facing a peculiar resonance because, by integrating in a single composite one component responsible for the sequestration of the carbon dioxide (sorbent) and one additive for the chemical conversion.[11] It allows the realization of more efficient apparatuses in terms of both chemical performance and energy consumption (Figure 1-lower). Among them, methanation strategies, dry reforming and reverse water gas shifts are among the most investigated strategies allowing the obtainment of energy vectors (methane, syngas and CO) efficiently, with the frequent use of metal-based catalysts.

Despite the elegance and large volumes of CO_2 treatable with these approaches, three main tasks still deserve attention to fulfil current sustainability criteria. The use of noble transition metals, the narrow portfolio of chemical CO_2 modifications (restriction to reductive processes) and compatibility issues of the sorbent/catalyst binary system still pose stimulating interrogatives to be tackled within the scientific community.

Here, in continuation with our recent research interests on graphene oxide (GO)-based carbocatalytic reactions,[12] and covalent modification of GO surfaces,[13] we recently documented on the efficiency of a fully organic GO - *L*-arginine (GO-Arg) composite in the interconversion of epoxides to cyclic carbonates *via* CO_2 insertion.[14] The electrophilic activation of carbon dioxide by the guanidinium unit of the amino acid[15] was documented as the pivotal chemical event for the final ring-expansion step. In addition, the effectiveness of organic amines as "sponges" in CO_2 capture methodologies is well consolidated.[16] However, despite the current operativity of several large-scale CO_2 capture facilities based on aqueous amine solution,[17] liquid-phase-amine strategies still face important shortcomings due to their corrosivity and sensitivity to nitrogen- as well as sulfur-based gasses. From here, the ongoing growing interest towards the developments of solid-phase-containing amine composites (supported amines materials) is recorded.

Therefore, we envisioned the possibility to combine key features of the GO-Arg composite such as trapping and chemical activation CO_2 towards the realization of an unprecedented reactive capture of CO_2 (RCC)[18] process by means of a fully organic dual function material (Figure 2).[19] Remarkably, this *proof-of-concept* model would address all the afore-described open tasks within ICCC strategies. Additionally, the application of ICCC to the valorization of CO_2 via C-O bond forming reactions would open new horizons in the preparation of added-value and structurally elaborated chemical compounds via direct CO_2 capture/fixation procedures.

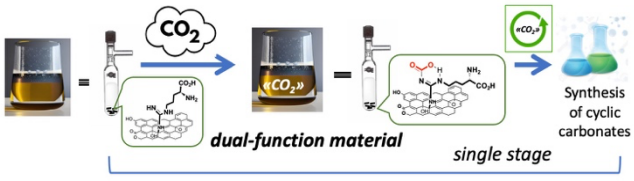

Figure 2. Graphical sketch of the present working hypothesis. Use of a dual functional material for a one-stage ICCC strategy.

Results and Discussion

Synthesis of the GO-Arg composites

The GO-Arg composites (GO-Arg 1:1; 1:3 and 1:5) were promptly synthetized by means of an adapted aminative procedure of GO surface.[20] In particular, aqueous suspensions of GO (100 mg, pH = 12 adjusted with NaOH) were treated with 100 mg, 300 mg and 500 mg of *L*-arginine (Arg), respectively. For purification, we exploited a home-made microfiltration strategy based on commercial Versatile PES© modules, (Plasmart 100 module, Medica Spa), featuring a cut-off module of 1000 KDa (ca. 150 nm) and with filtering surface of about 0.1 m^2.[21] Here, the employment of strongly basic aqueous solutions led to consider the guanidine unit most likely involved in the covalent grafting of arginine on the GO surface. However, a concomitant active role played by α-amino group cannot be excluded.

Conceptually, based on the side where the nucleophile approaches the GO surface, the reaction can generate a *syn*- or an *anti*-β-amino alcohol framework. In this context, we investigated the two stereodivergent mechanisms by means of QM/MM computations and the resulting potential energy surfaces (PESs) have been collected in Scheme 1.

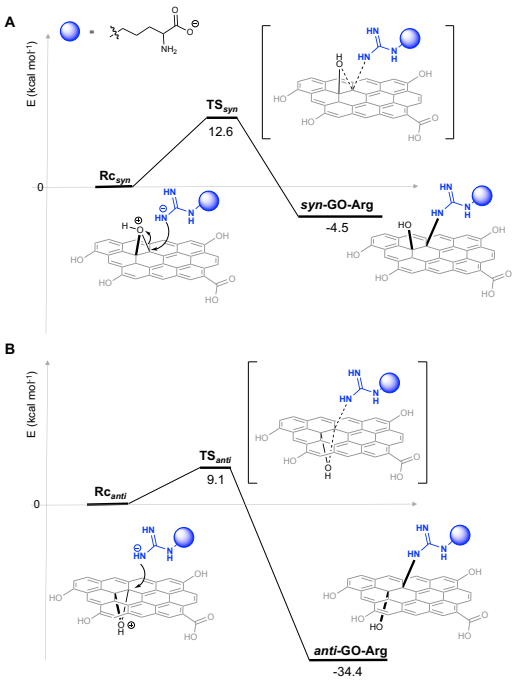

Scheme 1. PES obtained for the two possible stereodivergent mechanisms of β-amino alcohol formation upon *syn* (**A**) or *anti* (**B**) covalent grafting of arginine on GO *via* epoxide ring-opening: a) *syn*-attack. 2D-representation of the critical points are also inserted as insets.

Interestingly, both kinetic and thermodynamic parameters elected the *anti*-attack as most likely. In details, comparing the kinetics of the two mechanisms, the activation barrier for TS_{syn} is slightly higher than TS_{anti}, being 12.6 kcal mol^{-1} *vs* 9.1 kcal mol^{-1} in the case of the *anti*-attack.

Analogously, from a thermodynamic point of view, the formation of the *anti*-GO-Arg resulted strongly favored (-34.4 kcal mol^{-1}) respect to the *syn*-GO-Arg (-4.5 kcal mol^{-1}). Steric hindrance issues in the ring-opening product accounts for the aforementioned computations.

Subsequently, the superficial loading of arginine was experimentally determined *via* XPS analysis and in particular, the degree of surface decoration of GO was evaluated by monitoring the corresponding N 1s signals. As reported in Table 1 (see also SI for complete characterization), the materials presented an increasing atomic percentage of nitrogen as higher quantity of Arg was utilized in the synthesis. In particular, for GO-Arg 1:1 an atomic nitrogen content of 1.6% was recorded, this lifted up to 4.5% for GO-Arg 1:3. Differently, by further increasing the GO:Arg ratio up to 1:5 only a slight variation on nitrogen content was recorded (5.9%). Based on these outcomes, the estimated arginine loadings were 5%, 15% and 18%, respectively.

Table 1. Atomic compositions of the materials.[a]

Sample	C (%)	O (%)	N (%)	Arg loading (%)
GO-Arg (1:1)	84.3	14.4[b]	1.6	5.0
GO-Arg (1:3)	73.7	19.6	4.5	15.0
GO-Arg (1:5)	73.1	21.1	5.9	18.0

[a] Calculated by XPS analysis. [b] Relative loading of arginine in the materials obtained by considering the atomic ratios of *L*-Arginine (C:N:O = 6:4:2).

Thermal analyses

The CO_2 adsorption capacity of the dry GO-Arg samples with different arginine amounts was firstly measured by registering the mass change of the samples *via* TGA analysis upon CO_2 adsorption-desorption cycles. The adsorption/desorption curves are shown in Figure 3. The first part of the curve shows the cleaning cycle (*i.e.* desorption of any gaseous adsorbed species) at 90 °C performed in pure N_2 flux. The second part of the curve (yellow area) shows the absorption of CO_2 measured under a continuous CO_2/N_2 (1:1 v/v) stream, while the third part shows the CO_2 desorption at 90 °C in pure N_2. Each sample responds rapidly to the adsorption process due to the reaction between the arginine linked to GO and the carbon dioxide.

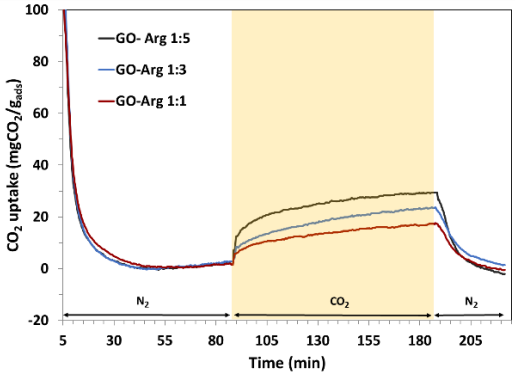

Figure 3. CO_2 adsorption/desorption curves of the Arg-functionalized GO samples with different Arginine amounts measured by TG analysis.

The extrapolated CO_2 uptake mean values for 1:1, 1:3, and 1:5 samples are reported in Table 2. These values increase with Arginine loading from the 1:1 (16.3 ± 0.8 mg g^{-1}) to the 1:5 sample (highest adsorption capacity of 28.2 ± 1.4 mg g^{-1}) due to the increased active sites of the material.

Table 2. CO_2 adsorption capacity of the arginine-functionalized GO samples.

Sample	CO_2 uptake ($mgCO_2$ / g adsorbent)[a]	CO_2 uptake static ($mgCO_2$ / g adsorbent)[b]
GO-Arg (1:1)	16.3 ± 0.8	20.1 ± 1.0
GO-Arg (1:3)	23.1 ± 1.1	26.5 ± 1.3
GO-Arg (1:5)	28.2 ± 1.4	39.3 ± 1.9

[a] Determined by TG analysis in flux of CO_2/N_2 mixture (1:1 % v/v). [b] CO_2 measured by TG analysis after absorption in static CO_2 (99.995%) for 2 h (further details in Supporting Information).

The same trend of adsorption was registered under pure static CO_2 absorption conditions (2 h, Table 2, see SI for details). The uptakes recorded using this method are higher than the ones reported for conventional TG analysis in flow due to the different operating conditions (*i.e.* GO-Arg 1:5, 39.3 ± 1.9 mg g^{-1}). Interestingly, the recorded CO_2 adsorption capacity of the GO-Arg (1:5) composite (ca. 1 mmol of CO_2 per gr of adsorbent) are in line with the reported adsorption values of amine-based materials for CO_2 trapping and utilization.[22]

The amount of adsorbed CO_2 was finally evaluated by monitoring the CO_2 desorption *via* thermogravimetric analysis. The curves representing the CO_2 desorption are reported (Figure S4). It is important to note that the desorption phenomena of the analysed samples are registered at the same temperature (around 70 °C) as reported in literature for similar amine functionalized materials[23] indicating a similar CO_2 absorption modes is operating in the different samples, regardless the arginine contents.

GO-Arg (1:5) sample was also considered to determine the CO_2 absorption in open air at room temperature. The absorption capacities measured using TG analysis after 1, 2, 3, 4 and 6 days were reported in Table 3 and Figure 4. The data show a nearly exponential increasing of the CO_2 uptake until the 4th day. After

this time, a stabilization of the uptake was observed at values of $mg_{CO2}/g_{adsorber}$ similar to the ones registered for the static absorption of the sample (see Table 2). It is important to note that the desorption occurred at the same temperature of the previous experiments (around 70 °C) as confirmation of the selective CO_2 absorption. Remarkably, these results emphasize the ability of the GO-Arg materials to selectively absorb the CO_2 present in the environment nevertheless its lower concentration.

Time (days)	CO_2 uptake ($mgCO_2$ / g $_{adsorber}$)[a]
1	24.0 ± 1.2
2	27.4 ± 1.4
3	31.6 ± 1.6
4	38.3 ± 1.9
6	38.7 ± 1.9

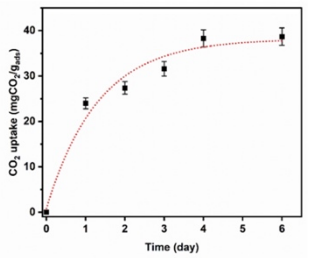

Figure 4. Left: CO_2 absorption capacity of the GO-Arg (1:5) sample left in open air (at room temperature). [a] CO_2 desorption measured by TG analysis after. The samples before the absorption (day 0) were subjected to a cleaning cycle at 90 °C for 30 min in pure N_2 flux to remove any gaseous adsorbed species. Right: graph of the CO_2 absorption capacity of the GO-Arg (1:5) in open air (rt) over time. The dotted red line represents the nearly exponential trend curve of the experimental data.

Due to the higher similarity between the analytical and experimental operative conditions for the successive transformation step (*vide infra*), the static CO_2 uptake was considered as the most reliable experiment for the calculation of the theoretical amount of CO_2 absorbed, to determine the conversions in the carbocatalytic processes.

Integrated CO_2 carbon capture and conversion.

The combination of our previous findings focused on the nucleophilic activation of CO_2 by GO-Arg and the previously established capability of GO-Arg to effectively trap carbon dioxide, led us to test this class of smart material for integrated CO_2 capture and chemical conversion. In this direction, we focused our attention on the synthesis of cyclic organic carbonates via CO_2-based ring opening of epoxides as a benchmark reaction.[24]

The synthesis of organic carbonates *via* CO_2 insertion represents an important synthetic strategy for large-scale production of long-vector organic scaffolds *via* a world-wide volume exceeding 100 ton/year. In this direction we set up a sequential one-pot CO_2 absorption – CO_2 conversion into cyclic carbonates always under the assistance of the GO-Arg composite. In particular, a "static" absorption period of CO_2 on dry GO-Arg was operated at 100 °C for 2 h. Then, consecutive N_2/vacuum cycles guaranteed the removal of the excess CO_2. The resulting [GO-Arg]/CO_2 adduct (vide infra) was then exposed to a solution of styrene epoxide (**1**) and TBAI in DMF under rigorous nitrogen atmosphere. Satisfyingly, under optimal conditions, carbonate **2** was formed proving the effectiveness of [GO-Arg]/CO_2 as a *reservoir* of activated "solid" CO_2 (Scheme 2).

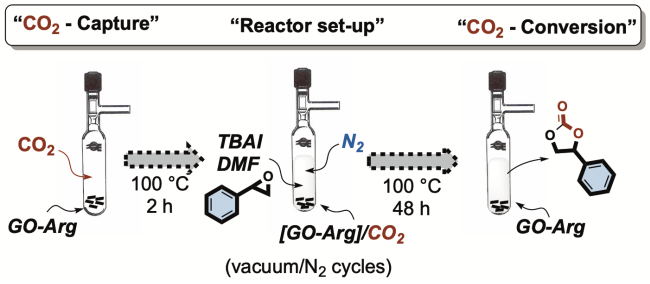

Scheme 2. Schematic representation of the integrated "capture-CO_2-conversion" strategy (TBAI: tetrabutylammonium iodide). During the capture stage, GO-based materials were exposed to ~ 0.7 mmol of CO_2 (99.9% purity).

The chemical yield (internal standard on NMR crude mixture) of the final cyclic carbonate **2** was determined by considering the maximal loading of CO_2 on the GO-Arg compounds determined by thermal analysis (see Table 2) and a collection of the resulting outcomes has been reported in Table 3. Interestingly, the previously reported GO-Arg (1:3) material proved efficiency in the two-stage one-pot approach by converting the 83% of the captured CO_2 into **2** (entry 5). Interestingly, all synthetized composites performed effectively in converting the trapped CO_2 into **2**. As a matter of fact, while GO-Arg 1:1 actively converted 60% of the trapped CO_2 (entry 4), the GO-Arg 1:5 analogues yielded carbonate **2** by utilizing 86% of the captured CO_2 (entry 6).

Table 3. Combined trapping and carbocatalytic conversion of CO_2 by GO-Arg composites.[a]

Run[a]	GO-Arg (x:x)	CO_2 adsorption	CO_2 conversion parameters	Yield of **2** (%)[b]
1	1:3	60 °C	optimal	27
2	1:3	optimal	16 h	29
3	1:3	optimal	60 °C	56
4	1:1	optimal	optimal	60
5	1:3	optimal	optimal	83
6	1:5	optimal	optimal	86
7	1:3	open air, rt, 24 h	optimal	75
8	1:3	vacuum, 50 °C. 2 h	optimal	20
9	1:3	optimal	DMSO	62
10	GO	optimal	optimal	traces
11	Arg	optimal	optimal	23[d]

12	1:3	optimal	optimal	NR[e]
13	-	optimal	optimal	NR[f]

[a] All attempts were carried out on/with a) adsorption stage: 40 mg of GO-Arg and ~ 0.7 mmol of CO_2 (99.9% purity), dry conditions for 2 h at 100 °C (closed) unless otherwise specified; b) conversion stage: 0.1 mmol of **1** (0.1 M) in reagent grade DMF for 48 h at 100 °C, unless otherwise specified. [b] Determined via ^{1}H NMR analysis of the reaction crude by means of the internal standard methodology (mesitylene). The theoretical amount of CO_2 absorbed on GO materials was considered as the limiting stoichiometry. [c] In the presence of recovered GO-Arg. [d] Calculated on styrene oxide as the limiting reagent. The reaction was carried out with 6 mg of Arg (estimated amount of Arg present in the GO-Arg 1:3 composite). [e] Without TBAI. [f] Without GO-Arg. NR: no reaction.

By electing the GO-Arg (1:3) as the model material, a range of different reaction parameters (*i.e.* time, temperature) were screened, (entries 1-3). However, both lower temperatures (stages 1 & 2) and shorter reaction time (stage 2) resulted in lower isolated yield of **2** with respect to the optimal conditions (entry 5). Moreover, based on the intriguing insights collected with the adsorption analyses carried out with air (Figure 4), we attempted an ICCC experiment simply exposing the GO-Arg for 24 h to a regular atmospheric mixture (adsorption stage). Interestingly, the material worked smoothly also under these conditions (yield of **2** = 75%), highlighting the potential applicability of the protocol towards selective CO_2 trapping/valorization of gas streams (entry 7). To corroborate the previous result, a blank experiment was performed by avoiding any CO_2 contamination of the material (entry 8). Here, albeit a residual amount of CO_2 was found in the freshly prepared GO-Arg (yield of **2** = 20%) the genuine role exerted by GO-Arg in sequestering CO_2 from the atmospheric mixture was accounted.

Furthermore, the synergistic roles of both GO and Arg components in the sequential process was proved by running the carbonate synthesis in the presence of GO and arginine as single promoters (entries 10 and 11). Here, while commercially available GO has been utilized in the *direct* CO_2 conversion to organic carbonates,[20] its implementation in a sequential protocol furnished disappointing outcomes (traces of **2**, entry 11). Interestingly, the use of unsupported arginine yielded **2** in 23% yield, proving the central role of the amino acid for the chemical activation of carbon dioxide. Finally, the synergistic action of both components GO-Arg and TBAI in promoting the ring-expansion of the epoxide (*vide infra* for mechanistic investigation) was stressed by the blank reactions exemplified in entries 12 and 13 in which implemented in absence of TBAI and GO-Arg respectively.

XPS studies: understanding the CO_2 absorption mode.

In our previous study, we postulated the covalent grafting of CO_2 on the GO-Arg surface (guanidine unit) though the formation of a carbamate group (**[GO-Arg]/CO_2,** Figure 6). To get more insights into this crucial aspect, XPS analyses were performed on the GO-Arg 1:3 sample before and after exposition to CO_2. For comparative purposes, an analogous investigation was also carried out on pristine GO (Figure S2 and Tables S9-11).

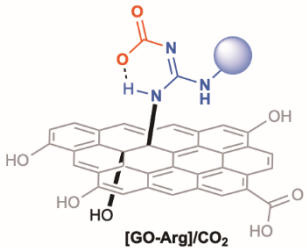

Figure 5. Structural representation of chemically activated CO_2 by GO-Arg composite.

The resulting photoemission peaks of C 1s, N 1s and O1 have been summarized in Figure 6 and Table 4 reports the binding energies and the percentages of the different contributions used to fit the photoemissions. In particular, the C 1s region was fitted including contributions from C=C sp^2, C-C sp^3, C-O+C-N, C-O-C, C=O+C=N, and O-C=O (for GO-Arg) and O-C=O+N-COO (for [GO-Arg]/CO_2).

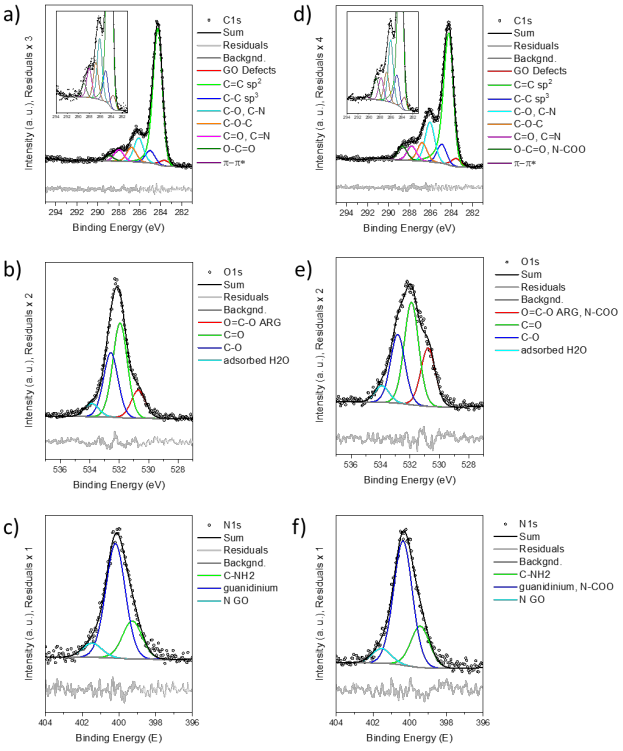

Figure 6. C 1s, O1s and N1s photoemission peaks and their fitting for GO-Arg (a, b, c) and for [GO-Arg]/CO_2 (d, e, f).

A contribution at lower BE (bonding energy) and a peak at higher BE account for GO defects and π-π* satellite interactions, respectively. O 1s region was fitted including four contributions deriving from C=O, C-O, adsorbed water and Arg carboxylic group and N-COO group for [GO-Arg]/CO_2. The BE (530.8 eV *ca.*) of the latter contribution agrees with a pure Arg sample used as reference compound (Figure S3). Moreover, pristine GO does not show this contribution at lower BE (Figure S2). It is important to

note that both in C 1s and O 1s regions of [GO-Arg]/CO_2, it is not possible to distinguish the peak of the carbamate group formed after the reaction with CO_2 as its binding energy is very similar to that of the carboxylic group of Arg.

On the other hand, C 1s and O 1s photoemission peaks show some relevant differences, when considering the relative amounts of the different contributions used to fit the raw data. In fact, O 1s of [GO-Arg]/CO_2 (Figure 6e) shows a larger amount (double) of the peak at 530.8 eV *ca.* ascribable at the O-C=O group of Arg and at the N-COO group formed after CO_2 treatment. Also, in the C 1s photoemission peak, the reaction with CO_2 implies a greater amount for the peak at 290 eV *ca.* that accounts for the O-C=O and N-COO groups (Figure 6d). Hence, XPS analyses strongly support the hypothesis that CO_2 is covalently trapped by GO-Arg thanks to the formation of a carbamate group (**Int3**) as depicted in Figure 7.

Finally, the N 1s photoemission peak was deconvoluted using two peaks with a 1:3 ratio as previously described (C-NH_2 and guanidinium group) and a third peak at higher BE due to GO-nitrogen interactions.[25] Here, a comparison between the pristine sample (Figure 6c) and the one exposed to CO_2 (Figure 6f) shows no appreciable differences. This is probably due to the fact that the guanidinium and the carbamate groups have very similar BE and XPS cannot resolve the two contributions.[26]

Table 4. BE and atomic percentage of the fitted C 1s, O 1s and N 1s photoemission peaks.

	GO-Arg		[GO-Arg]/CO_2	
	BE (eV)	at. %	BE (eV)	at. %
C1s				
defects	283.9	2.0	283.8	2.3
C=C	284.5	47.4	284.5	39.8
C-C	285.1	4.4	285.0	5.3
C-O, C-N	286.4	8.6	286.3	11.4
C-O-C	287.1	6.6	287.1	5.1
C=O, C=N	288.3	4.2	288.1	4.2
O-C=O, N-COO[a]	289.1	1.9	288.9	3.3
π-π*	291.2	0.5	291.0	0.8
O1s				
O-C=O Arg, N-COO[a]	530.7	2.5	530.8	5.1
C-O	531.9	6.0	531.9	5.9
C=O, C-O-C	532.7	8.2	532.9	8.9
adsorbed H_2O	533.9	1.2	534.0	1.4
N1s				
C-NH_2	399.3	1.1	399.4	1.2
Guanidinium, N-COO[a]	400.2	3.4	400.4	3.7
N in GO	401.5	0.4	401.5	0.4

[a] N-COO to be considered only for [GO-Arg]/CO_2.

Computational study

To elucidate the details of the reaction mechanism involved in the CO_2 activation and fixation reaction on GO-Arg, we carried out QM/MM computations. In this direction, we decided to investigate the reaction mechanism of CO_2 activation starting from the *anti*-complex to the formation of the carbonate **2** (**Pc**). Optimization of physiosorbed styrene oxide, iodine and CO_2 molecules generated the reactant complex (**Rc**), which corresponds to the asymptotic limit (**AL**) of the reaction. The PES reported in Figure 7 and the representation of the critical points of the MEP (minimum energy path) are shown as insets.

The overall reaction path that generates the final product can be divided into three main steps: 1) epoxide activation, 2) CO_2 activation, and 3) carbonate formation.

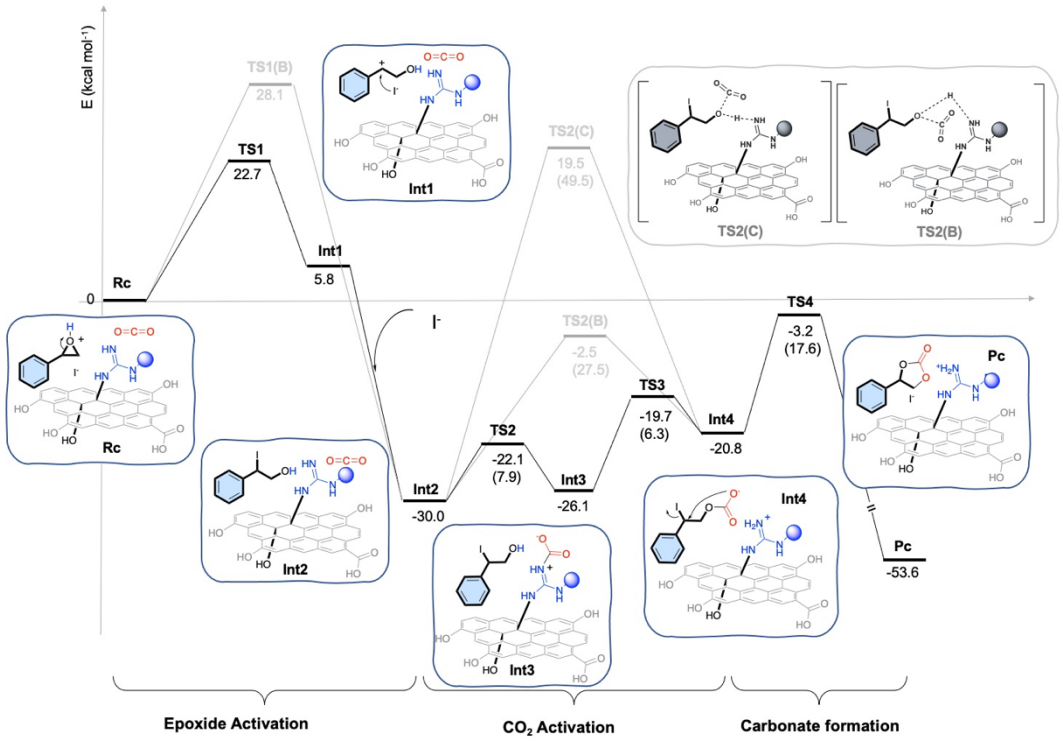

Figure 7. PES obtained for the CO_2 activation and fixation reaction catalyzed by arginine-grafted GO. 2D-representation of some of the critical points obtained for the CO_2 activation and fixation, are also inserted as insets.

Epoxide activation. The formation of the α-iodo-alkoxide intermediate **Int2** can follow either a S_N2 or a S_N1 mechanism. While the concerted mechanism requires 28.1 kcal mol^{-1} to occur, the transition state for the carbocation formation is located as 22.7 kcal mol^{-1}, suggesting that the reaction of epoxide-opening follows preferentially a S_N1 mechanism. The carbocation **Int1** (5.8 kcal mol^{-1} above **AL**), generated by the opening of the styrene oxide, collapses *via* a barrierless process, to the stable **Int2** by encountering the iodide ion (-30.0 kcal mol^{-1}). In both mechanisms (S_N2 and S_N1), the guanidinium group of the grafted arginine acts as an acid catalyst, protonating the epoxide group.

CO_2 activation. **Int2** can be converted into intermediate **Int4** by distinct reactive pathways depending on the role of the guanidium group of the grafted arginine: i) acid-base promoted mechanism, ii) electrostatic catalysis and iii) covalent CO_2 activation.

i) When the guanidium is not involved in any interaction with CO_2 (**TS2(C)**), it simply acts as a base (see Figure 7 inset-left), deprotonating the hydroxyl group of the α-iodo-alkoxide, activating the nucleophile for the reaction with CO_2. This process has an intrinsic activation barrier of 49.5 kcal mol^{-1}, *i.e.,* 19.5 kcal mol^{-1} above **AL**.

ii) In **TS2(B)** (Figure 7 inset-right), the guanidium interacts with CO_2 forming a bridge-like salt interaction, anchoring the carbon dioxide by forming two hydrogen bonds with its NH groups. In this geometry, CO_2 is slightly bent (O-Ĉ-O =160.5°) and more susceptible to the nucleophilic addition by the α-iodo-alkoxide: with respect to **TS2(C)**, the intrinsic activation energy lowers to 27.5 kcal mol^{-1}, laying at -2.5 kcal mol^{-1} below **AL**.

iii) The guanidium group can also bind carbon dioxide by forming a covalent bond. By overcoming **TS2**, which indicates a very fast process (7.9 kcal mol^{-1}), the carbamate intermediate **Int3**, that was spectroscopically identified by XPS analysis ([**GO-Arg/CO_2**]), is formed (-26.1 kcal mol^{-1}, N-C = 1.53 Å). On such intermediate, α-iodo-alkoxide easily attacks the electrophilic carbon of the activated CO_2, **TS3(C)** requiring only 6.3 kcal mol^{-1} to form **Int4**.

Considering the three possible reaction mechanisms that lead to the formation of **Int4**, the guanidinium group is crucial for the formation of an activated (*i.e.* bent) CO_2, that can undergo nucleophilic addition by α-iodo-alkoxide. This activation can take place *via* an electrostatic (**TS2(B**)) or a covalent (**TS2(C)**, **Int3**, **TS3**) catalysis, both allowed by the presence of the guanidium group grafted onto the GO surface. Regardless the type of mechanism, concomitantly with the formation of the carbamate-like intermediate **Int4**, the catalyst is restored in its positively charged form.

Carbonate formation. The last step of the reaction mechanism foresees the intramolecular closure of the carbonate into the cyclic carbonate product **Pc**. The negatively charged portion of

Int4 attacks intramolecularly the electrophilic carbon, bearing the iodine atom, with an activation barrier of 17.6 kcal mol^{-1}, so that **TS4** results to be only 3.2 kcal mol^{-1} below **AL.** Overall, the reaction generates a highly stable product (- 53.6 kcal mol^{-1}). It is worth mentioning that the overall mechanistic profile computed, and relative energy barriers agree with the optimal reaction parameters (**1** + CO_2 → **2**).

Recycling study

Finally, initial attempts to test the reusability of the GO-Arg in the process were carried out. Here, the material was recovered from the reaction mixture by filtration and upon simple washing/drying cycles (unoptimized recycling conditions), the GO-Arg 1:3 composite was employed in subsequent iterations (Scheme 3). Remarkably, although a drop in overall performance was recorded (II run: 54% yield and III run: 40% yield), these results support the present strategy for implementation into continuous/flow conditions.

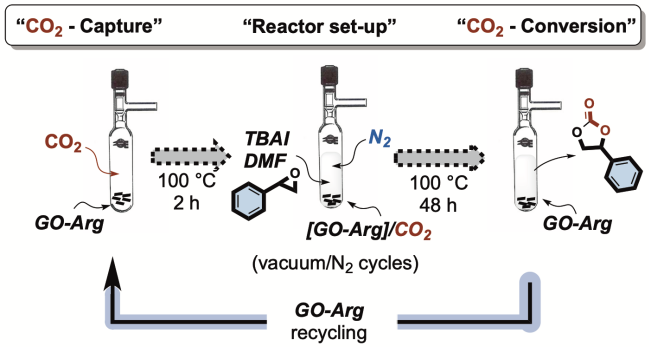

Scheme 3. Schematic representation of the iterative ICCC strategy. The recycling stage involved simple filtration/washing/dryness iterations of the recovered GO-Arg.

Conclusion

A dual function class of organic materials is documented for the direct trapping and chemical valorization of carbon dioxide. The readily available graphene oxide-arginine composite enabled the selective sequestration of CO_2 from gas streams, including atmospheric air, and its concomitant chemical activation towards the incorporation to cyclic carbonates. Adsorption properties were investigated *via* dedicated thermal analysis and XPS spectroscopy investigation unambiguously proved the covalent anchoring of CO_2 into the material surface via formation of reactive carbamates. Finally, computations were carried out to shed light on the stereochemical profile of the initial covalent modification of the GO material and provided a rationale for the whole chemical transformation [CO_2 → cyclic carbonates].

Supporting Information

General procedure for the tandem CO_2 fixation/carbocatalysis. An oven-dried Schlenk tube was charged with 40 mg of GO-Arg material, and the nitrogen atmosphere was converted into CO_2 by means of three vacuum-CO_2 cycles. The mixture was led stirring for 2 h at 100 °C. After cooling, the CO_2 was evacuated and the Schlenk tube filled with N_2. Subsequently, 1 mL of dry DMF, 0.01 mmol of racemic styrene oxide (12.5 μL) and 37 mg of TBAI (0.01 mmol) were added in a sequence. The reaction mixture was stirred at 100 °C for 48 h and the insoluble GO removed by filtration and washed with EtOAc.

CO_2 adsorption measurements. The CO_2 adsorption capability of samples was determined *via* Thermogravimetric Analysis (TGA, STA449 F3 Jupiter Thermo-Microbalance, Netzsch-Gerätebau) considering both a) in flux and b) static CO_2 absorptions. The samples, weighed into a Al_2O_3 crucible, were subjected to an initial cleaning cycle at 90 °C for 30 min (heating rate: 10 °C min^{-1}) in a high-purity nitrogen atmosphere (99.999%) before the absorption of CO_2 to ensure the desorption of any adsorbed gaseous species that could reduce the adsorption capability of the samples. In the method a) a 100 minutes-long CO_2 isothermal adsorption cycle (40 °C) under a CO_2/N_2 mixture (1:1 v/v) was set after the cooling samples from 90°C to 40 °C (cooling rate: 1 °C min^{-1}, N_2). Finally, the temperature was increased to 90°C (heating rate: 10 °C min^{-1}) in pure N_2 for the final desorption step. In the method b) the crucible filled with desorbed material was placed in a closed glass vessel filled with pure CO_2 (99.995%) and let at 40 °C for 2 hours to ensure the CO_2 adsorption. After this time, the crucible was placed again in the TGA apparatus for the final desorption cycle at 90 °C (heating rate: 10 °C min^{-1}) in pure N_2 (similar to what reported for the method a)) to evaluate the amount of desorbed CO_2.
By measuring the mass change during the TGA analysis (absorption for the method a) and desorption for the method b)), CO_2 uptake values were calculated and expressed as $mg_{CO2}/g_{adsorbent}$.

Computational Details. All computations were carried out employing a hybrid approach based on quantum mechanical and molecular mechanical (QM/MM) theory, through the ONIOM formalism,[27] as implemented in the Gaussian16 software.[28] A two-layer approach was adopted, where the high layer (*i.e.*, the reactive species) is treated at DFT level, employing the M06-2X functional, which has already been reported to accurately describe the energetic of carbocatalytic reactions,[29] in combination with the 6-31+G* basis set for C, H, O and N atoms, while 3-21G* for I. The lower layer (*i.e.*, the graphene basal plane) was treated using the UFF force field.[30] All critical points were fully optimized, and their nature was investigated by frequency calculations, which confirmed the presence of only positive eigenvalues for minima, and only one negative eigenvalue for transition states.

Acknowledgements

Acknowledgments are made to University of Bologna and Consorzio CINMPIS are kindly acknowledge for financial support. MB is also grateful to the PRIN-2017 project 2017W8KNZW for the financial support. ESCALAB QXi Spectrometer was funded by “Sviluppo delle infrastrutture e programma biennale degli interventi del Consiglio Nazionale delle Ricerche (2019).”

Keywords: Carbon-capture-conversion • Graphene oxide • Computational study • Carbon dioxide • Spectroscopic investigation

[1] a) H. Ritchie, M. Roser "CO_2 and Greenhouse Gas Emissions". *Published online at OurWorldInData.org.* Retrieved from: 'https://ourworldindata.org/co2-and-other-greenhouse-gas-emissions', **2017**; b) A.A. Lacis, G.A. Schmidt, D. Rind, R.A. Ruedy, *Science*, **2010**, *330*, 356; c) N. Mac Dowell, P.S. Fennell, N. Shah, G.C. Maitland, *Nature Climate Change* **2017**, *7*, 243.

[2] M. Coccia, *Sustainable Futures* **2023**, *5*, 100114.

[3] M.N. Anwar, A. Fayyaz, N.F. Sohail, M.F. Khokhar, M. Bagar, A. Yasar, K. Rasool, A. Nazir, M.U.F. Raja, M. Rehan, M. Aghbashlo, M. Tabatabaei, A.S. Nizami, *J. Env. Management* **2020**, *260*, 110059.

[4] a) A. Goeppert, M. Czaun, G. K. Surya Prakash, G. A. Olah, *Energy Environ. Sci.*, **2012**, *5*, 7833; b) M.E. Boot-Handford, J.C. Abanades, E.J. Anthony, M.J. Blunt, S. Brandani, N. Mac Dowell, J.R. Fernandez, M.C. Ferrari, R. Gross, J.P. Hallett, R.S. Haszeldine, P. Heptonstall, A. Lyngfelt, Z. Makuch, E. Mangano, R.T.J. Porter, M. Pourkashanian, G.T. Rochelle, N. Shah, J.G. Yao, P.S. Fennell, *Energy Environ. Sci.,* **2014**, *7*, 130; c) Y. Tan, W. Nookuea, H. Li, E. Thorin, J. Yan, *Energy Convers. Manag.* **2016**, *118*, 204.

[5] S. Rezaei, A. Liu, P. Hovington, *Cat. Today*, **2023**, *423*, 114286.

[6] C. Ehlig-Economides, M.J. Economides, *J. Petrol. Sci. Eng.* **2010**, *70*, 123.

[7] M. Liu, L. Zhan, Y. Wang, X. Zhaio, J. Wu, D. Deng, J. Jiang, X. Zheng, Y. Lei, *J. Mat. Sci. Tech.* **2023**, *165*, 235, and references therein.

[8] For general reviews, see: a) M.E. Boot-Handford, J.C. Abanades, E.J. Anthony, M.J. Blunt, S. Brandani, N. Mac Dowell, J.R. Fernández, M.C. Ferrari, R. Gross, J.P. Hallett, R.S. Haszeldine, P. Heptonstall, A. Lyngfelt, Z. Makuch, E. Mangano, R.T.J. Porter, M. Pourkashanian, G.T. Rochelle, N. Shah, J.G. Yao, P.S. *Energy Environ. Sci.* **2014**, *7*, 130; b) c) E. Daneshvar, R. J. Wicker, P. L. Show, A. Bhatnagar, *Chem. Eng. J.* **2022**, *427*, 130884; d) S. Chen, J. Liu, Q. Zhang, F. Teng, B. C. McLellan, *Renew. Sust. Energ. Rev.* **2022**, *167*, 112537.

[9] A. Goeppert, M. Czaun, J.-P. Jones, G.K.S. Prakash, G.A. Olah, *Chem.Soc.Rev.* **2014**, *43*, 7995.

[10] a) J. Chen, Y. Xu, P. Liao, H. Wang, H. Zhou, *Carbon Capture Sci. Technol.* **2022**, *4*, 100052; b) B. Shao, Y. Zhang, Z. Sun, J. Li, Z. Gao, Z. Xie, J. Hu, H. Liu, *Green Chem. Eng.* **2022**, *3*, 189; c) B. Shao, Z.-Q. Wang, X.-Q. Gong, H. Liu, F. Qian, P. Hu, J. Hu, *Nat. Commun.* **2023**, *14*, 996.

[11] a) S. Kar, A. Goeppert, G.K.S. Prakash, *Acc. Chem. Res.* 2019, **52**, 2892; b) W. Zhang, Y. Tang, Y. Li, F. Li, M. Luo, *Materials Today Catal.* **2023**, *2*, 100006.

[12] a) L. Favaretto, J. An, M. Sambo, A. De Nisi, C. Bettini, M. Melucci, A. Kovtun, A. Liscio, V. Palermo, A. Bottoni, F. Zerbetto, M. Calvaresi, M. Bandini, *Org. Lett.* **2018**, *20*, 3705; b) L. Lombardi, D. Bellini, A. Bottoni, M. Calvaresi, M. Monari, A. Kovtun, V. Palermo, M. Melucci, M. Bandini, *Chem. Eur. J.* **2020**, *26*, 10427; c) L. Lombardi, M. Bandini*, Angew. Chem., In. Ed.* **2020,** *59,* 20767; d) A. Brunetti, A. Pintus, L. Lombardi, A. Kovtun, F. Mascietti, F. Bruno, E. Ravera, M. Melucci, G. Bertuzzi, M. Bandini, *Chin. J. Chem.* **2023**, *41*, 1333; e) S. Mantovani, A. Pintus, A. Kovtun, G. Bertuzzi, M. Melucci, M. Bandini, *Eur. J. Org. Chem.* **2023**, e202300641.

[13] L. Lombardi, A. Kovtun, S. Mantovani, G. Bertuzzi, L. Favaretto, C. Bettini, V. Palermo, M. Melucci, M. Bandini, *Chem. Eur. J.* **2022**, *29*, e202200333.

[14] A. Pintus, S. Mantovani, A. Kovtun, G. Bertuzzi, M. Melucci, M. Bandini, *Chem. Eur. J.* **2023**, *29*, e202202440.

[15] S.Y. Huang, J. Ma, J.P. Li, N. Zhao, W. Wei, Y.H. Sun, *Catal. Commun.* **2008**, *9*, 276; b) J. Ma, X. Zhang, N. Zhao, A.S.N. Al-Arifi, T. Aouak, Z. A. Al-Othman, F. Xiao, W. Wei, Y. Sun, *J. Mol. Cat. A: Chem.* **2010**, *315*, 76; c) H. M. Lee, I. S. Youn, M. Saleh, J.W. Lee, K.S. Kim, *Phys. Chem. Chem. Phys.* **2015**, *17*, 10925; d) Y. Yoshida, N. Aoyagi, T. Endo, *Beilstein J. Org. Chem.* **2018**, *14*, 2204; e) Y. Mao, X. Yang, T.V. Gerven, *Environ. Sci. Technol.* **2023**, *57*, 10816.

[16] For general reviews see: a) S.P. Sreejyothi, S.K. Mandal, *Chem. Sci.* **2020**, *11*, 10751; b) R. Ramezani, S. Mazinani, R. Di Felice, *Rev. Chem. Eng.* **2022**, *38*, 273. See also c) Z.-Z. Yang, L.-N. He, Y.-N. Zhao, B. Li, B. Yu, *Energy Environ. Sci.* 2011, **4**, 3971; d) A.-H Liu, R. Ma, C. Song, Z.-Z. Yang, A. Yu, Y. Cai, L.-N.; He, Y. Zhao, B. Yu, Q.-W. Song, *Angew. Chem. Int. Ed.* 2012, **51**, 11306-11310; e) J. Kothandaraman, A. Goeppert, M. Czaun, G.A. Olah, G.K.S. Prakash, *Green Chem.* 2016, **18**, 5831

[17] Global CCS-Institute, 2019, The Global Status of CCS, 2019, Australia.

[18] R.E. Siegel, S. Pattanayak, L.A. Berben, *ACS Catal.* **2023**, *13*, 766.

[19] a) N. Hsan, P.K. Dutta, S. Kumar, J. Koh, *J. CO_2 Util*. **2022**, *59*, 101958. For examples of amino and metal functionalized GO/*r*GO with implications on CO_2 conversion into cyclic epoxides and carbamates, see: b) V.B. Saptal, T. Sasaki, K. Harada, D. Nichio-Hamane, B.B. Bhanage, *ChemSusChem* **2016**, *9*, 644 and c) X. Zhang, K.-H. Chen, Z.-H. L.-N. He, *ChemCatChem* **2020**, *12*, 4825.

[20] a) S. Khabnadideh, E. Mirzaei, L. Amiri-Ziretol, *J. Mol. Struct.* **2022**, *1261*, 132934; b) I.A. Vacchi, C. Spinato, J. Raya, A. Bianco, C. Ménard-Moyon, *Nanoscale*, **2016**, *8*, 13714; c) C. Martin, A. Ruiz, S. Keshavan, G. Reina, D. Murera, Y. Nishina, B. Fadeel, A. Bianco, *Adv. Funct. Mat.* **2019**, *29*, 1901761; d) I.A. Vacchi, S. Guo, J. Raya, A. Bianco, C. Ménard-Moyon, *Chem. Eur. J.* **2020**, *26*, 6591.

[21] a) S. Mantovani, S. Khaliha, L. Favaretto, C. Bettini, A. Bianchi, A. Kovtun, M. Zambianchi, M. Gazzano, B. Casentini, V. Palermo, M. Melucci, *Chem. Commun.* **2021**, *57*, 3765; b) S. Mantovani, S. Khaliha, T. D. Marforio, A. Kovtun, L. Favaretto, F. Tunioli, A. Bianchi, G. Petrone, A. Liscio, V. Palermo, M. Calvaresi, M.L. Navacchia, M. Melucci *Chem. Commun.* **2022**, *58*, 9766.

[22] L.B. Hamdy, C. Goel, J.A. Rudd, A.R. Barron, E. Andreoli, *Mater. Adv.* **2021**, *2*, 5843, and references therein.

[23] a) A. R. Sujan, D. R. Kumar, M. Sakwa-Novak, E. W. Ping, B. Hu, S. J. Park, C. W. Jones, *ACS Appl. Polym. Mater.* **2019**, *11*, 3137; b) F. Zarei, P. Keshavarz, *Sep. Purif. Technol.* **2023,** *323* 124438

[24] a) A.J. Kamphuis, F. Picchioni, P.P. Pescarmona, *Green Chem.* **2019**, *21*, 406; b) P.P. Pescarmona, *Curr. Opin. Green Sustain. Chem.* **2021**, *29*, 100457.

[25] a) J.- Zhu, S. Wang, Y. Gu, B. Xue, Y. Li, *Mat. Chem. Phys.* **2018**, *208*, 68; b) S. Zhang, H. Zhang, F. Cao, Y. Ma, Y. Qu, *ACS Sustainable Chem. Eng.* **2018**, *6*, 4204; Y. He, Y. Xia, J. Zhao, Y. Song, L. Yi, L. Zhao, *Appl. Phys. A* **2019**, *125*, 160.

[26] a) J.S. Stevens, A.C. de Luca, M. Pelendritis, G. Terenghi, S. Downes, S.L.M. Schroeder, *Surf. Interface Anal.* **2013**, *45*, 1238; b) A. Artemenko, A. Shchukarev, P. Štenclová, T. Wågberg, J. Segervald, X. Jia, A. Kromka, *IOP Conf. Ser.: Mater. Sci. Eng.* **2021**, 012001.

[27] a) S. Dapprich, I. Komàromi, K. S. Byun, K. Morokuma, M. J. Frisch, *J. Mol. Structure Theochem* **1999**, *21,* 461; b) T. Vreven, K. S. Byun, I. Komàromi, S. Dapprich, J. A. Montgomery, Jr. K. Morokuma, and M. J. Frisch, *J. Chem. Theory Comput.* **2006**, *2*, 815.

[28] M. J. Frisch, G. W. Trucks, H. B. Schlegel, G. E. Scuseria, M. A. Robb, J. R. Cheeseman, G. Scalmani, V. Barone, G. A. Petersson, H. Nakatsuji, X. Li, M. Caricato, A. V. Marenich, J. Bloino, B. G. Janesko, R. Gomperts, B. Mennucci, H. Hratchian, J. V. Ortiz, A. F. Izmaylov, J. L. Sonnenberg, F. Ding, F. Lipparini, F. Egidi, J. Goings, B. Peng, A. Petrone, T. Henderson, D. Ranasinghe, V. G. Zakrzewski, J. Gao, N. Rega, G. Zheng, W. Liang, M. Hada, M. Ehara, K. Toyota, R. Fukuda, J. Hasegawa, M. Ishida, T. Nakajima, Y. Honda, O. Kitao, H. Nakai, T. Vreven, K. Throssell, J.A. Montgomery Jr., J. E. Peralta, F. Ogliaro, M. J. Bearpark, J. J. Heyd, E. N. Brothers, K. N. Kudin, V. N. Staroverov, T. A. Keith, R. Kobayashi, J. Normand, K. Raghavachari, A. P. Rendell, J. C. Burant, S. S. Iyengar, J. Tomasi, M. Cossi, J. M. Millam, M. Klene, C. Adamo, R. Cammi, J. W. Ochterski, R. L. Martin, K. Morokuma, O. Farkas, J. B. Foresman, D. J. Fox, Gaussian 16 Rev. C.01, Wallingford, CT, **2016**.

[29] a) T. D. Marforio, A. Bottoni, P. Giacinto, F. Zerbetto, M. Calvaresi, *J. Phys. Chem. C.* **2017**, *121*, 27674; b) T. D. Marforio, A. Bottoni, F. Zerbetto, M. Calvaresi, *ChemNanoMat* **2019**, *4*, 499; c) T. D. Marforio, M. Tomasini, A. Bottoni, F. Zerbetto, E. J. Mattioli and M. Calvaresi, *Nanomaterials*, **2023**, *13*, 8.

[30] A. K. Rappé, C. J. Casewit, K. S. Colwell, W. A. Goddard III, W. M. Skif, *J. Am. Chem. Soc.* **1992**, *114*, 10024.

Entry for the Table of Contents

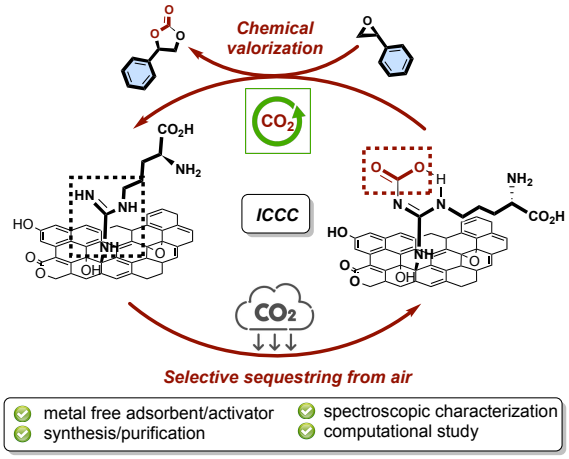

Efficient dual function materials for ICCC are proposed. A family of graphene oxide-arginine composites enabled the “on-demand” selective trapping and efficient release of CO_2 via incorporation into cyclic carbonates. Thermal analyses, XPS investigations and computational studies revealed the adsorbent properties of the material as well as the covalent chemical one-pot sequestration/activation mode operated on CO_2.

Researcher Twitter usernames: @M_BANDINI_GROUP.